

# HiSST: 4th International Conference on High-Speed Vehicle Science Technology

22 -26 September 2025, Tours, France



# Design Optimization of the Launch System for the Scramjet Hypersonic Experimental Vehicle (SHEV)

F. Cascone<sup>1</sup>, P. Roncioni<sup>1</sup>, V. Paolella<sup>1</sup>, A. Vitale<sup>1</sup>, M. Marini<sup>1</sup>, S. Di Benedetto<sup>1</sup>, S. Cardone<sup>2</sup>, M. Albano<sup>3</sup>, R. Bertacin<sup>3</sup>

#### **Abstract**

This paper presents the comprehensive redesign and optimization of the launch system for the Scramjet Hypersonic Experimental Vehicle (SHEV), conducted within an Italian national project, supported by the national research program PRO.R.A. and the Italian Space Agency (ASI). The primary objective of this redesign was to address significant aerodynamic, structural, and stability challenges identified in the original launch vehicle (LV) configuration. Critical issues included high aerodynamic loads, complex structural interfaces, difficulties in maintaining aerodynamic stability, and safe separation dynamics between the SHEV and LV at hypersonic speeds. The redesigned configuration incorporates an optimized aerodynamic nose-tip, a repositioned wing structure, enhanced tail placement and scale, and a refined positioning of the SHEV relative to the booster. Aerodynamic assessments by means of Eulerian CFD simulations demonstrated substantial improvements in aerodynamic efficiency and reductions in drag. Stability and trimmability analyses confirmed significant enhancements in both longitudinal and lateral-directional stability throughout the flight trajectory. Interface analyses between the LV and SHEV showed reduced mechanical complexity and improved reliability, facilitating safer and more precise payload separations. Preliminary trajectory evaluations indicated effective load management under anticipated flight conditions, further confirming the robustness of the new design. Comparative analyses highlighted notable advancements over the original configuration, particularly improved aerodynamic stability margins, reduced structural loads, and enhanced maneuverability. Overall, the redesigned LV configuration substantially improves mission reliability and effectiveness, marking a significant advancement towards the practical development of hypersonic propulsion technologies and setting a foundation for future operational hypersonic vehicle missions.

**Keywords**: Hypersonic Flight, Aerodynamic Optimization, Scramjet Propulsion, Launch System Optimization, Aerodynamic Database.

#### **Nomenclature**

 $Cl\beta$  – rolling moment coefficient derivative

Cma – pitching moment coefficient derivative

Cnβ – yawing moment coefficient derivative

 $Cy\beta$  – side force coefficient derivative

CoG – Centre of Gravity

LV - Launch Vehicle

M - Mach number

M<sub>A</sub> – aerodynamic pitching moment

M<sub>T</sub> – pitching moment due to thrust

SHEV - Scramjet Hypersonic Experimental Vehicle

T – thrust

a – angle of attack

β – angle of sideslip

δe – elevon deflection

 $\varepsilon_T$  – thrust vectoring

FPA, γ – flight path angle

<sup>&</sup>lt;sup>1</sup> CIRA, Italian Aerospace Research Center, via Maiorise 81043, Capua (CE), Italy, f.cascone@cira.it.

<sup>&</sup>lt;sup>2</sup> TecnoSistem, vico II S. Nicola alla Dogana, 80133, Naples, Italy.

<sup>&</sup>lt;sup>3</sup> ASI, Italian Space Agency, via del Politecnico snc, 00133 Rome, Italy. HiSST-2025-132



# HiSST: 4th International Conference on High-Speed Vehicle Science Technology

22 -26 September 2025, Tours, France



#### 1. Introduction

The present paper contributes to the ongoing development of advanced hypersonic propulsion technologies through an Italian national project, aimed at establishing a robust national capability in hypersonic flight. This project aligns with various European initiatives over recent decades, including LAPCAT I&II, ATLLAS I&II, FAST20XX, HIKARI, HEXAFLY, HEXAFLY-INT, and STRATOFLY, as well as national developments such as the French ZEHST aircraft and the UK's SKYLON vehicle. Despite these substantial efforts, hypersonic civil transport has historically faced challenges in terms of range limitations due to high fuel consumption. However, recent advancements in integrated propulsion and aerodynamics, notably in LAPCAT-II and STRATOFLY configurations, have provided promising pathways to overcoming these issues ([1], [2], [3], [4]).

The goal of the present project is to design a propelled vehicle capable of sustained, controlled flight at hypersonic speeds (Mach 6÷8) and altitudes between 27 and 32 km. The original configuration of the flight demonstrator, named SHEV, encountered substantial challenges, especially related to aerodynamic stability, structural loads, and interface dynamics under hypersonic conditions. These complexities highlighted the necessity of a comprehensive redesign aimed at significantly improving the vehicle's performance, reliability, and overall mission success.

This paper provides a detailed analysis of the rationale behind the redesign, outlining specific modifications that have been integrated to enhance aerodynamic efficiency and stability. Major adjustments included refining the aerodynamic nosetip, repositioning the wing structure for optimal aerodynamic performance, scaling and enhancing tail placement, and strategically repositioning the SHEV relative to the booster to increase the fineness ratio. Eulerian CFD simulations played a crucial role in verifying these aerodynamic enhancements, demonstrating clear improvements in performance metrics such as reduced drag and increased stability.

Further, this work encompassed extensive stability and trimmability analysis to confirm the effectiveness of the redesigned configuration throughout the expected flight envelope. Comprehensive interface evaluations were also conducted to streamline the mechanical complexity and ensure safer, more predictable payload separation under demanding hypersonic flight conditions. Preliminary trajectory analyses have been pivotal in assessing the structural loads experienced throughout the mission, demonstrating robust performance even under high-stress scenarios.

The comparative analyses presented in this paper clearly illustrate the considerable benefits achieved with the redesigned configuration over the original system. These benefits include enhanced aerodynamic stability, significant reductions in structural loads, improved maneuverability, and optimized integration between SHEV and LV components.

Future directions of this research will involve further detailed viscous CFD simulations, in-depth investigations of maneuver dynamics, particularly regarding the optimization of the roll maneuver, and comprehensive mechanical interface studies. Collectively, these activities aim to further refine and validate the launch system design, ensuring its readiness for practical hypersonic vehicle missions and contributing valuable insights toward the future of hypersonic propulsion technology.

#### 2. Mission and System Description

The preliminary mission concept envisages an air-launched solution with a carrier (stage I) capable of releasing the payload, composed by the propelled hypersonic demonstrator and the launch vehicle equipped with a booster, at a target point in terms of speed and altitude. From here the launch vehicle

accelerates until it reaches the foreseen trajectory target point in terms of Mach and altitude, where the hypersonic propelled demonstrator is released and the scramjet must work for a time of 10 seconds.

It is therefore possible to identify four mission phases (Fig 1):

Phase 1: Ascent of the carrier aircraft with the payload;

**Phase 2**: from the release of the payload from the carrier to the release of the demonstrator at the target point;

Phase 3: Experimental window (10 s);

**Phase 4**: Gliding phase.

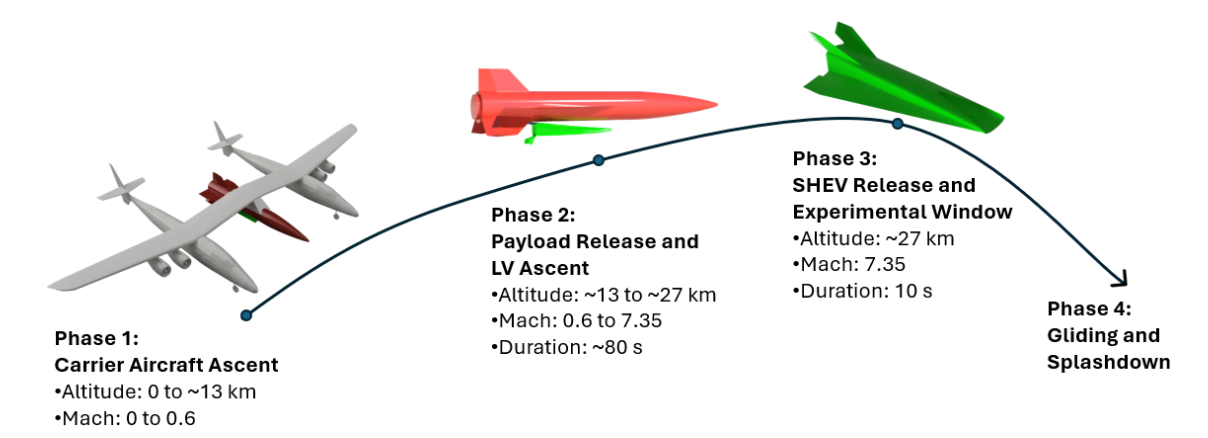


Fig 1. Mission Scenario

The launch vehicle connected to the propelled hypersonic demonstrator is represented in Fig 2.



Fig 2. Payload configuration (left) and SHEV (right)

The configuration of the propelled hypersonic demonstrator is based on the concept of "waverider", or a hypersonic vehicle with high aerodynamic efficiency in supersonic regime obtained through the exploitation of shock waves that form on the lifting surfaces, a phenomenon known as "compression lift". The demonstrator must also include a scramjet air-breathing propulsion system. The concept is depicted in Fig 2, and is a heritage of the already studied EU-FP7 HEXAFLY (see refs [5], [6], [7]).

# 3. Launch Vehicle Design Optimization

The original design of the launch vehicle [10] presented several challenges that significantly impacted on the aerodynamic performance, structural integrity, and interface complexity between the SHEV and LV. One of the primary concerns identified in the original configuration was the occurrence of excessively high aerodynamic loads, particularly pronounced during ascent phases at low supersonic conditions. These loads not only influenced structural sizing and weight but also complicated the mechanical interface, introducing risks during critical separation maneuvers. Moreover, the previous configuration required additional structural wedges at the SHEV-LV interface, further increasing mechanical complexity and mass. To address these critical issues comprehensively, a detailed Page | 3

multidisciplinary optimization approach was adopted, focusing specifically on aerodynamic refinement, structural simplification, and enhanced overall system reliability.

More specifically, placing the SHEV ahead of the launcher generated large bending moments (cantilever-like), necessitating numerous support rods and a complex interface. Part of this hardware would have remained attached to the SHEV during the experiment, increasing drag and shortening the test for a given fuel load. Moreover, the forward SHEV position constrained the launcher nose length, producing a strong forebody shock and degrading LV performance.

Repositioning the SHEV under the launcher effectively resolves these issues. The new layout drastically reduces bending moments thanks to a much shorter moment arm; primary loads are now mainly due to SHEV drag. Consequently, this allows for a simplified interface that remains entirely attached to the LV after SHEV separation, eliminating residual components on the experimental vehicle and improving aerodynamic efficiency. We are currently evaluating several possible interfaces. Fig 3 shows one of the solutions that we are currently evaluating.

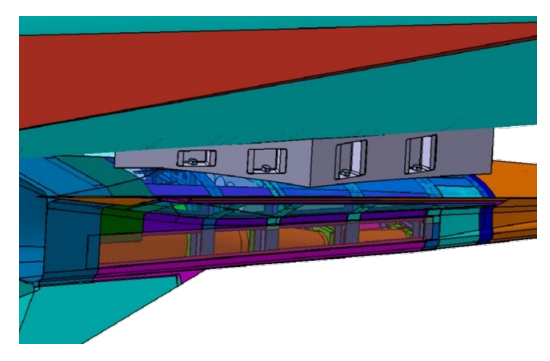
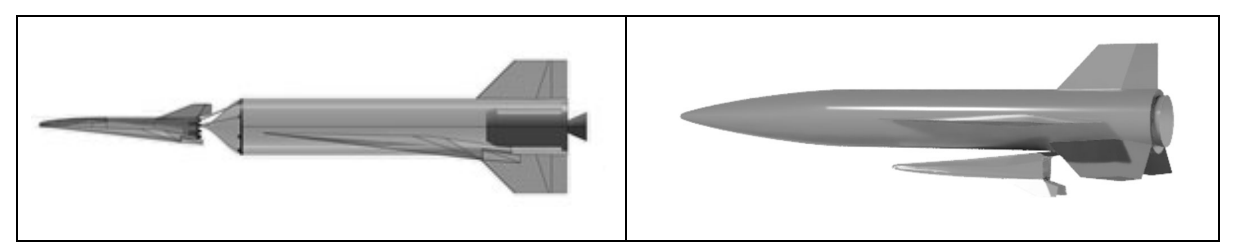


Fig 3. Diamond shape interface with 8 M30 pyrobolts

Additionally, this revised positioning enables a longer and more aerodynamically efficient nose for the launcher, resulting in a weaker conical shock wave, significantly enhancing performance compared to the initial configuration (Fig 4).

However, the major drawback of this new configuration lies in the complexity of the SHEV release maneuver. Since the SHEV is positioned inverted under the belly of the launcher, a roll maneuver is required during ascent to position the SHEV atop the LV or, alternatively, executed by the SHEV after separation (this last option is currently considered riskier and still not explored). Future work will specifically address ensuring rapid and safe separation dynamics post-release.



**Fig 4.** Examined structural configurations of the payload: SHEV and launch vehicle in line (left) and SHEV under launch vehicle (right)

#### 4. Aerodynamic Database Building and Results

The Aerodynamic DataBase (AEDB) gathers the complete set of aerodynamic data as global/local forces, moments, and pressure distributions over the vehicle. It includes: (i) force and moment components versus key flight variables (Mach, Re,  $\alpha$ ,  $\beta$ , control deflections, etc.); and (ii) surface pressure maps. These data feed flight-mechanics and structural analyses. The final AEDB will be established through a combination of numerical simulations and experimental activities.

This paper focuses on the preliminary study and aerodynamic characterization of the Payload (the scramjet hypersonic demonstrator coupled to the launch vehicle), which corresponds to the second phase of the mission (Fig 1).

The activities results are reported in terms of:

- Numerical aerodynamic database built by means of Inviscid CFD simulations for the clean configuration of the Payload (LV + SHEV);
- Control surfaces effect.

In this section will be described the operations performed in order to obtain the Aerodynamic Database (AEDB) for the Payload which will be useful for conducting flight mechanics analyses ([8] and [9]). The aerodynamic database is provided as a function of Mach number ( $M_{\infty}$ ), angle of attack (a) and the elevon deflections ( $\delta_e$ ). However, the analysis does not consider the effect of sideslip angle ( $\beta$ ). The reference quantities are reported in Table 1. The location of the Centre of Gravity is strongly variable due to the consumption of the burning solid grain of the booster.

Reference Length (L <sub>ref</sub> )	4.1248 m
Reference Surface (S <sub>ref</sub> )	4.7936 m <sup>2</sup>
Mass	17000 kg

**Table 1.** Reference Quantities

# 4.1. Clean configuration

The calculation of the aerodynamic coefficients for the clean configuration of the Payload has been obtained by means of inviscid CFD simulations. The simulations have been carried out using the commercial code ANSYS FLUENT®. Each solution is assumed to be convergent when the residuals drop more than three orders of magnitude, and the aerodynamic coefficients reach a constant value. The reference quantities (Table 1) considered for these calculations are the same already used for the SHEV, in order to obtain aerodynamic coefficients that are easily comparable with those already calculated for the demonstrator.

The computational grids (Fig 5) have been generated using the ICEMCFD® software. The unstructured grids have about 10 million cells (for half configuration).

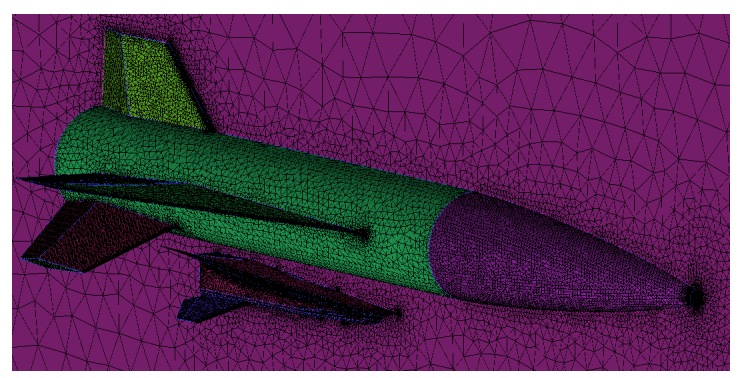


Fig 5. Calculation grid for Payload inviscid simulations

In addition, an adaptive mesh based on a density gradient criterion was employed in near the nose, between the LV – SHEV interface (the interface wall is not present in these simulations), and inside the SHEV nozzle, in order to capture the shock wave position varying Mach number and AoA.

The Payload aerodynamic coefficients as a function of Mach number and AoA are summarized in Fig 6 and in Fig 7.

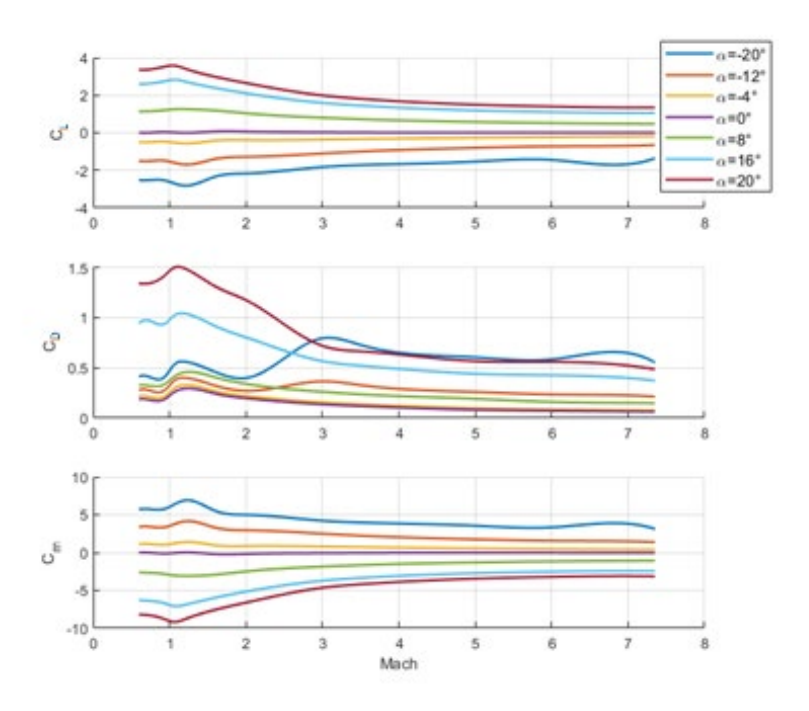


Fig 6. Aerodynamic coefficients as a function of Mach number, for different AoA

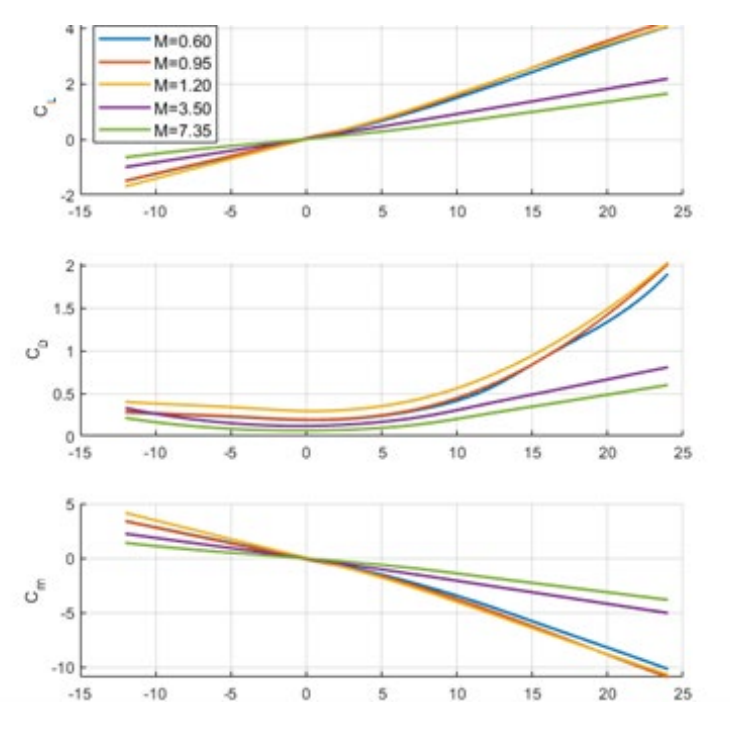


Fig 7. Aerodynamic coefficients as a function of AoA, for different Mach numbers

It is important to notice that the pitching moment coefficients displayed in Fig 6 and in Fig 7 are calculated with respect to the LV nose (X = Y = Z = 0 m). The coefficients reported in these figures are representative of the AEDB and characterize the aerodynamics of the LV taking into account the approximations made. Despite the complexity of the system, no particularly relevant characteristics emerge, except for transonic conditions where the coefficients undergo strong variations (as expected). For what concerns the LV, the CoG is varying over time due to the burning of the solid propellant, therefore it is not possible to evaluate its longitudinal stability without an in-depth mission

analysis. Despite this, for illustrative purposes, Fig 8 shows the  $C_M$  relative to the CoG position estimated at the moment of ignition of the solid propellant (x about 9.35 m behind the SHEV nose).

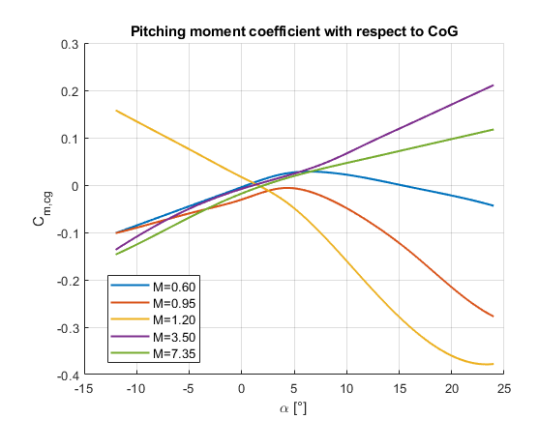


Fig 8. Pitching moment coefficient relative to CoG, as a function of AoA, varying Mach number

Then, assuming a linear variation of the Mach number with increasing altitude, it was possible to apply a viscous correction [10] to the drag coefficient. In this way it is possible to take into account the increase in drag due to viscosity.

#### 4.2. Control Surfaces Effect

The effect of elevon deflection was quantified once in the previous work [10] on the SHEV and is reused here in compact form. Inviscid CFD was performed on a simplified model (wing + elevon) to compute the variation of the aerodynamic coefficients with respect to the undeflected case. The resulting increments were defined as:

$$\Delta C_X(\delta_e) = C_X(\delta_e) - C_X(\delta_e = 0), \quad X \in \{L, D, M\}$$
 (1)

For the LV, the elevon increments were obtained by scaling the SHEV elevon coefficients with the ratio of the elevon wetted areas. The pitching-moment increment is scaled not only by the elevon area ratio but also by the ratio of the elevon moment arms, measured from the same reference point:

$$\Delta C_X^{LV} = \Delta C_X^{SHEV} \frac{S_{e,LV}}{S_{e,SHEV}}, \quad X \in \{L,D\} \quad \text{and} \quad \Delta C_M^{LV} = \Delta C_M^{SHEV} \frac{S_{e,LV}}{S_{e,SHEV}} \cdot \frac{d_{e,LV}}{d_{e,SHEV}}$$
(2)

The final deliverable of this analysis is a set of lookup tables of  $\Delta C_L$ ,  $\Delta C_D$  and  $\Delta C_M$  that can be superimposed to the clean AEDB to obtain trimmed conditions or to run flight-mechanics analyses without re-running CFD for each deflection.

#### 4.3. Comparison with old configuration

The redesigned configuration significantly enhances aerodynamic performance by simplifying the mechanical interface between the SHEV and the launch vehicle (LV), allowing for a more extended LV nose. Previously, the forward positioning of the SHEV severely limited the nose length of the LV, generating a strong, nearly-normal shock wave immediately ahead of the LV. This intense shock wave dramatically increased aerodynamic drag, significantly degrading system efficiency. With the SHEV repositioned beneath the LV, the launcher now features an elongated aerodynamic nose profile, generating a much weaker, oblique shock wave. Consequently, this modification substantially reduces overall aerodynamic drag, as clearly indicated by comparative CFD simulations.

The aerodynamic comparison conducted at a constant angle of attack ( $AoA = 4^{\circ}$ ) across various Mach numbers highlights noteworthy improvements (Fig 9). Although the new configuration shows slightly reduced lift, due to the inverted position of the SHEV below the LV and due to the removal of the wing incidence angle, which is now symmetric. The reduction in aerodynamic drag is considerably greater. As a result, aerodynamic efficiency (CL/CD ratio) improves dramatically, achieving efficiency gains up

to 3 at high Mach numbers compared to the original configuration. These aerodynamic enhancements directly contribute to improved mission performance, enabling more effective payload delivery and optimized use of fuel resources during ascent and hypersonic experimentation phases.

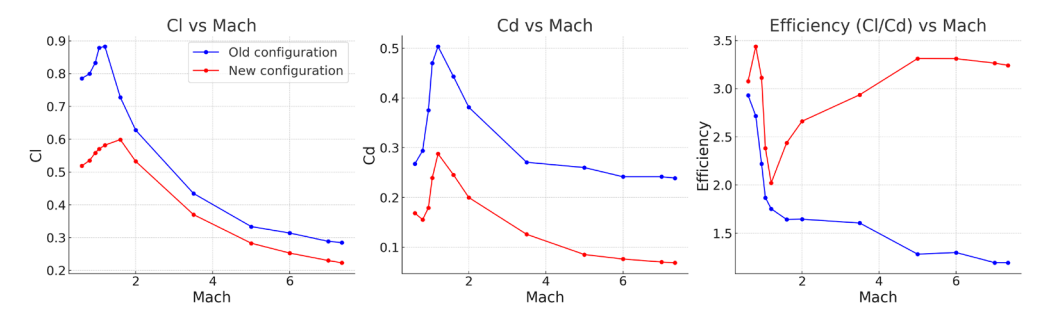


Fig 9. Comparison of CL, CD and efficiency between old and new configurations, for AoA = 4° varying Mach

# 5. Aerodynamic Characterization

#### 5.1. Longitudinal Trimmability and Stability assessment

Starting from the AEDB, it is possible to verify the trimmability and stability of the Payload configuration under certain assumptions.

Assuming the thrust trend of the Orion 50 ST [10] and considering also the possible use of the rocket with thrust vectoring (TV) control ( $\pm 5^{\circ}$  as declared by supplier), and the variation of the mass over the time (varying due to the burning of solid propellant, as shown in Fig 10), it is therefore possible to perform a preliminary check on flyability of the Payload.

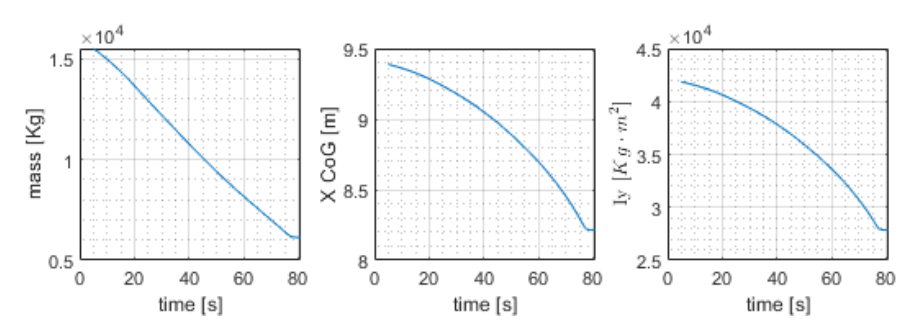


Fig 10. Mass, CoG and longitudinal inertia variation over the time for Payload

Starting from the release of the payload from the carrier (M  $\approx$  0.6, altitude  $\approx$  13 Km, Sep1 in Fig 1), knowing the aerodynamic characteristics of the payload as a function of M, AoA and  $\delta_e$ , and considering the assumptions done in the previous section, it is possible to make a preliminary check of the Payload trimmability. It is possible to do that for each Mach number, finding the couples of AoA and  $\delta_e$  that trim the Payload (root of the following system of equations):

$$\begin{cases} mV \frac{d\gamma}{dt} = T \cdot \sin(\alpha + \varepsilon_T) + L(M, \alpha, \delta_e) - W \cdot \cos\gamma \\ M_A(M, \alpha, \delta_e) + M_T = 0 \end{cases}$$
 (3)

The two equations of the system 3 are coupled, and their solution allow us to get the AoA and elevon for known conditions. Then, it is possible to update the velocity and the altitude by solving the following equations:

$$m\frac{dV}{dt} = T \cdot \cos(\alpha + \varepsilon_T) - D(M, \alpha, \delta_e) - W \cdot \sin\gamma$$
 (4)

$$\frac{dh}{dt} = V \cdot \sin \gamma \tag{5}$$

Eq. 5 represents the update of altitude over the time, useful to update the dynamic pressure (International Standard Atmosphere model has been assumed). The thrust vectoring angle has been assumed variable in order to guarantee a trimming condition for each Mach number.

A practical approach to solve these equations is to impose the flight path angle (FPA,  $\gamma$ ) at each time step and subsequently determine the corresponding angle of attack (AoA), elevon deflection angle ( $\delta$ e), and thrust vectoring angle ( $\epsilon$ T) that guarantee the vehicle follows the prescribed  $\gamma$ (t). Essentially, this method involves specifying a desired trajectory profile and computing the trim conditions required to maintain it. Each time step is treated independently since the primary objective is to identify instantaneous trim conditions rather than simulating a continuous trajectory evolution. Nevertheless, to ensure continuity, at each instant the selected trim solution will be the closest possible to the conditions found at the previous time step. Currently, the main goal is to confirm that at least one valid trim condition exists for every instant throughout the mission and to ensure that these conditions are longitudinally stable. Detailed trajectory analysis, involving full dynamic evolution, will be the subject of future investigations.

The adopted approach to define the  $\gamma(t)$  curve was to impose an analytical shape, which was subsequently optimized. Specifically, the FPA profile was defined by two third-degree polynomial curves subjected to various constraints and including only two degrees of freedom that allowed optimization. The rationale behind employing two cubic functions for the FPA is based on the expected flight trajectory of the vehicle after payload release. Initially, the launcher must execute a pull-up maneuver, characterized by a convex  $\gamma(t)$  profile. Subsequently, it transitions into a pull-down maneuver to achieve a levelled flight condition with zero angle of attack, resulting in a concave  $\gamma(t)$  profile. Thus, once the two cubic curves were established (Fig 11) along with several boundary conditions, such as zero slope at the start of the first curve and at the end of the second curve, as well as continuity and tangency constraints between the two curves, only two free parameters remained:

- The tangency point  $\mathbf{t}_m$  between the two curves, corresponding to the time instant at which  $\gamma(t)$  reaches its maximum value;
- The value of  $\gamma(t)$  at this tangency point,  $\gamma_m$  (i.e. the maximum FPA during the ascent trajectory).

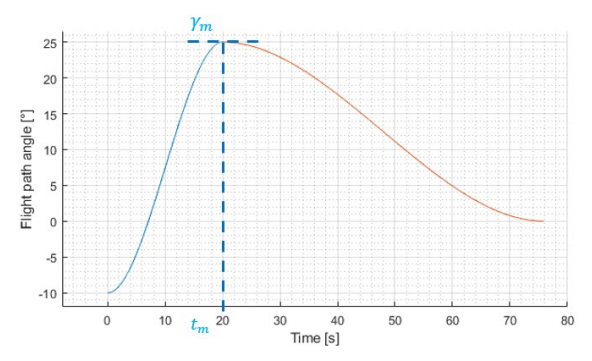


**Fig 11.** Example of  $\gamma(t)$  shape to be optimized

A multi-objective optimization was therefore performed, varying these two parameters to optimize the final Mach number, the final altitude reached, and minimize the peak structural load at interface during the ascent. This approach results in a  $\gamma_m$  of approximately 22, after 40 seconds from the start of the ascent Fig 12.

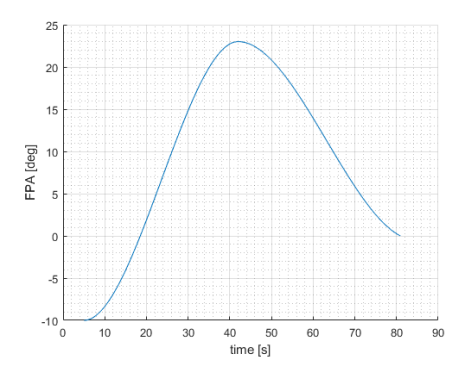


**Fig 12.** Optimized y(t) curve

Once the optimized FPA profile was defined, trim conditions along the trajectory could be computed, as described previously. In this analysis, it was assumed that the roll maneuver occurs instantaneously during ascent, approximately at 40 seconds into the flight, specifically when the angle of attack reaches zero. However, as previously mentioned, the timing of the roll maneuver has not yet been finalized. Alternative scenarios include performing the roll maneuver immediately after release from the carrier aircraft or just prior to the SHEV separation. Detailed flight mechanics analyses are currently underway to determine the most advantageous timing and approach for the roll maneuver.

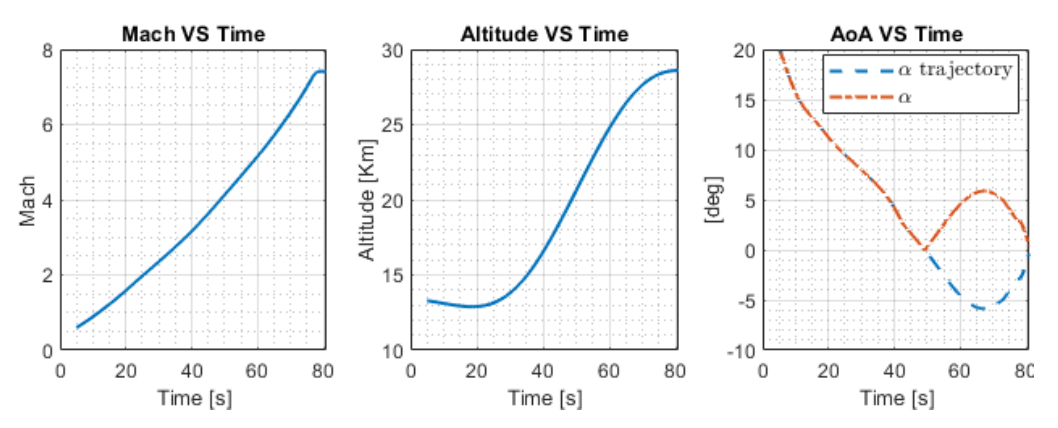
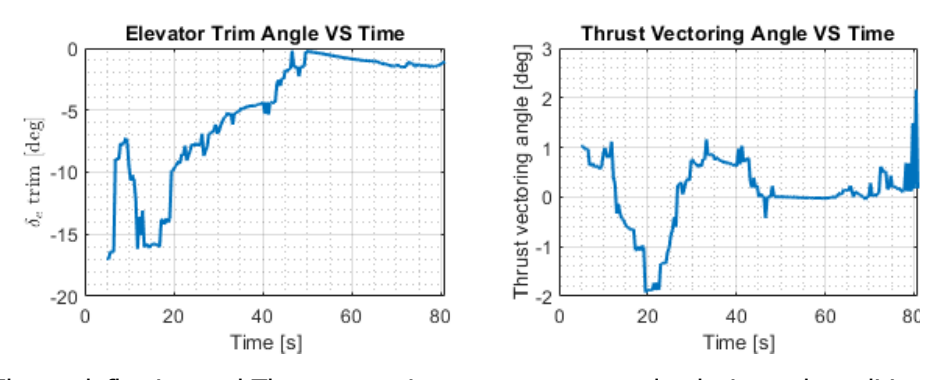


Fig 13. Payload trimmed conditions for each timestep



**Fig 14.** Elevon deflection and Thrust vectoring to guarantee payload trimmed conditions for each timestep

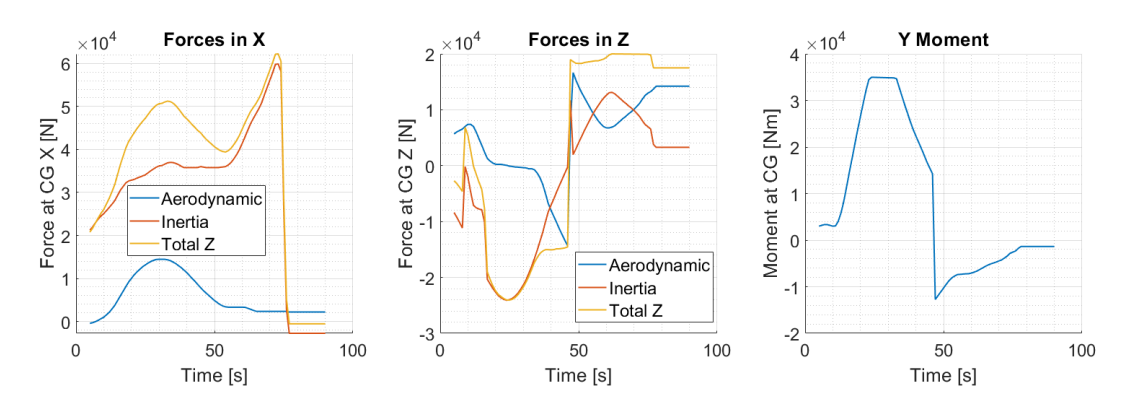
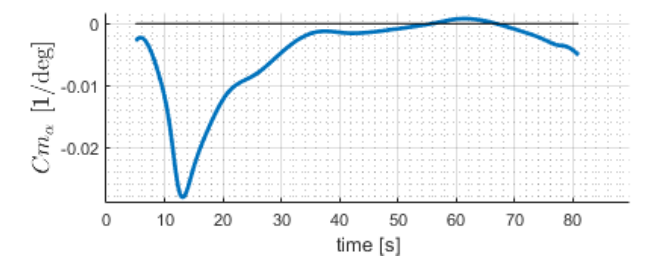


Fig 15. Loads at SHEV CoG during ascent

The preliminary results shown in Fig 13, Fig 14 and Fig 15 allow us make some considerations:

- 1. With the assumptions made, the altitude and Mach number for the demonstrator test can be reached;
- 2. For low Mach number, a very high AoA should be considered to obtain a trimmed condition, due to the dynamic pressure still too low;
- 3. For each flight condition, an AoA exists that trims the Payload (however, it depends on  $\gamma(t)$  and  $\varepsilon_T(t)$ );
- 4. The final altitude is depending on  $\gamma(t)$ . The shown trajectory brings to an altitude greater than 28 Km. However, modifying  $\gamma(t)$  does not impact significantly the final Mach number;
- 5. The elevon deflection angle required to maintain trim varies between -17° and +1°, while the thrust vectoring angle never exceeds 5°, in line with the supplier's specification. It is important to reiterate that these trim conditions depend on the assumptions made: the center of gravity position over time (which may shift), the chosen Flight Path Angle profile, and the limitations of the current model, which focuses on identifying instantaneous trim conditions rather than simulating a continuous trajectory evolution. Moreover, multiple trim solutions can exist at each time instant; the primary goal of this preliminary analysis was to verify that at least one feasible trim solution exists for every instant throughout the mission profile.
- 6. The loads are evaluated with respect to the SHEV CoG and will be used for the preliminary sizing of the interface. They are significantly lower than those of the previous configuration and are therefore considered manageable. These values do not include the roll maneuver; however, the loads induced by that maneuver are expected to be much smaller than those shown here.

Finally, for each instantaneous trim condition (i.e., for each Mach number and AoA along the prescribed trajectory), the slope of the pitching moment coefficient (Cm) curve with respect to AoA is evaluated about the CoG. Ensuring that this slope remains negative (Fig 16) confirms that each identified trim condition also satisfies the longitudinal stability requirement.



**Fig 16.** CM $\alpha$  for each instant of the ascent trajectory

#### 5.2. Lateral-Directional Stability assessment

A further check that can be done on the launch system is the presence of lateral and directional static stability; this condition is expressed in terms of derivatives as following:

$$\frac{dc_y}{d\beta} < 0$$
,  $\frac{dc_n}{d\beta} > 0$  and  $\frac{dc_l}{d\beta} < 0$ . (6)

Where  $C_l$  is the Rolling moment coefficient, and is positive when right wing is down;  $C_n$  is the yawing moment coefficient, and is positive when right wing is backward;  $C_Y$  is the side force coefficient and is positive when the force is pushing on the left side of the vehicle toward the right.

Preliminary inviscid CFD calculation will be made on the full configuration for some Mach number between 0.6 and 7.35 with a sideslip angle ( $\beta$ ) of 4°, for both zero AoA and the one expected by longitudinal analysis for each Mach number. For example, from the longitudinal analysis, a high AoA is expected for the trim at lower Mach number (about 20°), so this AoA will be used for lateral and directional analysis at low Mach number.

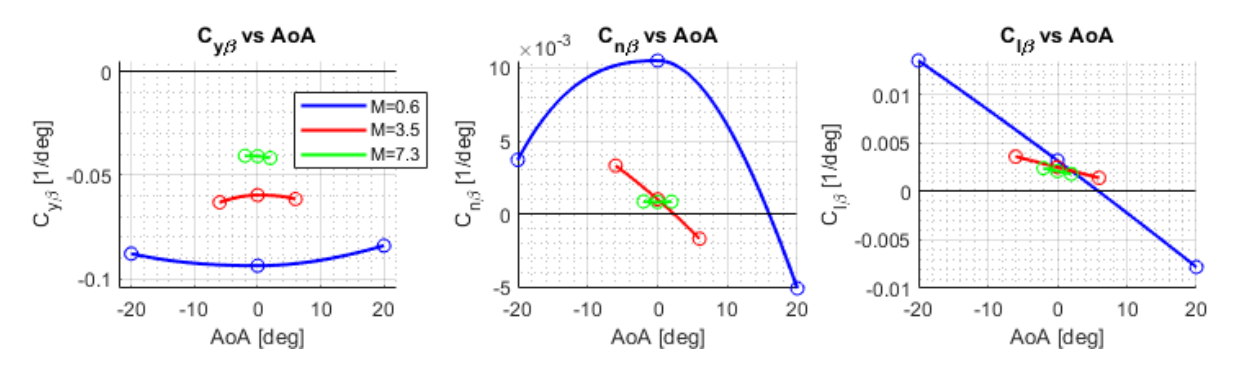


**Fig 17.** Derivatives for lateral-directional stability: Cy $\beta$  (left), Cn $\beta$  (center) and Cl $\beta$  (right)

From the results shown in Fig 17, we can derive the following conclusions:

- 1. The side force coefficient derivative Cy $\beta$  is always negative;
- 2. The yawing moment coefficient derivative  $Cn\beta$ , remains positive across most flight conditions, except at low Mach numbers and high angles of attack. However, at high AoA the strong coupling between roll and yaw dynamics means it is more accurate to consider the dynamic derivative  $Cn\beta^*$ , which also depends on the unknown moments of inertia ( $I_{xx}$  and  $I_{zz}$ ). It is expected that this enhanced derivative will improve the overall directional stability, so the region where  $Cn\beta$  briefly becomes negative does not pose a critical issue.
- 3. The roll moment coefficient derivative Clβ, appears positive (indicating instability) across most flight conditions. Indeed, this derivative will change sign following the roll maneuver. Additionally, the current analysis assumes the center of gravity lies along the LV's longitudinal axis, which is not strictly true (the lateral offset of the SHEV shifts the overall CoG). Consequently, this derivative does not pose a critical issue either. However, it may become a useful constraint when determining the timing for the roll maneuver needed to position the SHEV above the launcher.

#### 6. Conclusions

The present study has successfully addressed critical aerodynamic and interface issues through a comprehensive redesign of the Launch Vehicle (LV) configuration for the Scramjet Hypersonic Experimental Vehicle (SHEV). The initial configuration, characterized by excessive structural complexity and reduced aerodynamic performance due to the forward positioning of the SHEV, has been significantly improved. Repositioning the SHEV under the LV effectively reduced bending moments at interface and allowed for a simplified interface design that remains entirely attached to the LV after payload separation. Consequently, this configuration significantly decreases aerodynamic drag by enabling a more aerodynamically efficient, elongated nose on the launcher, resulting in substantially weaker shock and improved overall performance.

Aerodynamic analyses conducted using Eulerian CFD have confirmed notable enhancements in aerodynamic efficiency, achieving up to a threefold improvement in efficiency across various Mach numbers. The trimmability analysis verified that the redesigned configuration provides feasible trim solutions throughout the entire mission envelope. Longitudinal stability and Lateral-Directional stability have been assessed without significant criticalities.

Future work will focus on several key areas to further validate and enhance the redesigned LV configuration:

- Viscous CFD Analysis: perform comprehensive viscous computational fluid dynamics simulations to more accurately characterize aerodynamic forces, including real-gas and thermal effects, to further refine aerodynamic predictions.
- Flight-Mechanics Simulation: carry out a full 6-DOF flight-mechanics analysis by numerically integrating the rigid-body equations of motion with time-varying mass and inertia properties, coupled to actuator (TV/elevon) dynamics and aerodynamic/propulsive models.
- Roll Maneuver: conduct detailed studies to identify optimal timing and dynamics for the roll
  maneuver, ensuring rapid orientation adjustments and minimizing the risk during SHEV
  separation.
- Mechanical Interface Validation: evaluate and validate the robustness of the redesigned mechanical interface through dedicated structural analyses, ensuring safe and reliable payload separation under operational conditions.

Although it has not been elaborated in this paper, activities and tests on the SHEV are also underway in parallel.

#### **Acknowledgements**

The work has been co-funded by Italian Space Agency and CIRA ScPA in the frame of the agreement nr. 2022-13-HH.0-F43D22000410005.

#### References

- J. Steelant, R. Varvill, C. Walton, S. Defoort, K. Hannemann, M. Marini, "Achievements Obtained for Sustained Hypersonic Flight within the LAPCAT-II Project", AIAA-2015-3677, 20th AIAA International Space Planes and Hypersonic Systems and Technologies Conference, July 06-09, 2015.
- 2. E. Blanvillain, G. Gallic, "HIKARI: Paving the way towards High Speed Air Transport", *AIAA-2015-3676, 20th AIAA International Space Planes and Hypersonic Systems and Technologies Conference*, July 6-9, 2015.
- 3. Mack A., Steelant J., Adirim H., Lentsch A., Marini M., Pilz N., "FAST20XX: Achievements on European Suborbital Space Flight", *7th European Symposium on Aerothermodynamics*, Brugge, Belgium, May 2011.
- 4. J. Steelant et al., "Achievements obtained within ATLLAS-II on Aero-Thermal Loaded Material Investigations for High-Speed Vehicles", 21st AIAA International Space Planes and Hypersonics Technologies Conference, 6-9 March 2017, China.
- 5. J. Steelant et al., "Conceptual Design of the High-Speed Propelled Experimental Flight Test Vehicle HEXAFLY", AIAA-2015-3539, *20th AIAA International Space Planes and Hypersonic Systems and Technologies Conference*, Glasgow, Scotland, U.K., July 6-9, 2015.
- 6. G. Pezzella, M. Marini, M. Cicala, A. Vitale, T. Langener, J. Steelant, "Aerodynamic

- Characterization of HEXAFLY Scramjet Propelled Hypersonic Vehicle", *AIAA-2014-2844, AIAA Aviation, 32nd AIAA Applied Aerodynamics Conference*, 16-20 June 2014, Atlanta, GA, USA.
- 7. Di Benedetto S., Di Donato M.P., Schettino A., Scigliano R., Nebula F., Morani G., Cristillo D., Marini M., Cardone S., Steelant J., Villace V., "The high-speed experimental flight test vehicle of HEXAFLY-INT: a multidisciplinary design", CEAS Space Journal, published online on 5 January 2021, DOI: 10.1007/s12567-020-00341-5.
- 8. Roncioni P., Vitagliano P. L., De Gregorio F., Pezzella G., Romano L., Paglia F., "Aerodynamic Appraisal of the VEGA-C Launcher", *JSR-Journal of Spacecraft and Rockets*, 24 April 2023, http://arc.aiaa.org | DOI: 10.2514/1.A35610.
- 9. Viola N., Roncioni P., Gori O., Fusaro R., "Aerodynamic Characterization of Hypersonic Transportation Systems and Its Impact on Mission Analysis", *MDPI-Energies*, 16 June 2021, https://doi.org/10.3390/en14123580.
- 10. Cascone F., Roncioni P., Russo O., Marini M., Di Benedetto S., Albano M., Bertacin R., Ranuzzi G., *Launch System Assessment of an Experimental Hypersonic Scramjet Vehicle*, Proceedings of ICAS 2024 International Council of the Aeronautical Sciences, 2024.